Surface Residence and Uptake of Methyl Chloride and Methyl Alcohol at the Air/Water Interface Studied by Vibrational Sum Frequency Spectroscopy and Molecular Dynamics†

Kandice Harper,‡ Babak Minofar,§,|| M. Roxana Sierra-Hernandez,‡ Nadia N. Casillas-Ituarte,‡ Martina Roeselova,*,|| and Heather C. Allen*,‡

Department of Chemistry, The Ohio State University, 100 West 18th Avenue, Columbus, Ohio 43210, Institute of Physical Biology, University of South Bohemia, Zamek 136, Nove Hrady, Czech Republic, and Institute of Organic Chemistry and Biochemistry, Academy of Sciences of the Czech Republic, Flemingovo nam. 2, 16610 Prague 6, Czech Republic

Received: September 29, 2008; Revised Manuscript Received: December 10, 2008

Vibrational sum frequency generation (VSFG) spectroscopy and molecular dynamics (MD) simulations are used to study the surface residence and organization of gas-phase methyl halide and methyl alcohol molecules adsorbed to the air/water interface, while Raman spectroscopy is used to detect the uptake of the gas-phase species into the bulk aqueous phase. Spectroscopy results reveal the presence of methyl alcohol in the bulk and at the surface. Methyl chloride is detected in the bulk, but not at the surface. This indicates that methyl alcohol adsorbs to the aqueous surface in a layer that is ordered, in agreement with previous studies, and is also readily taken up into the bulk aqueous phase, whereas methyl chloride adsorbs, but, while being taken up into the bulk liquid, has lower surface number density and/or forms a more disordered surface layer than methyl alcohol. MD simulations show that methyl halide molecules transition readily between the gas phase and interface, resulting in significantly shorter residence times at the surface for the methyl halides relative to methyl alcohol. Both the geometries that the methyl species adopt at the interface and the interactions between the methyl species and the interfacial water molecules differ for the halides and the alcohol. Complementary studies of butyl species show similar results: butyl alcohol adsorbs to the aqueous surface in a layer that exhibits a certain degree of order corresponding to the chains aligned along the surface normal, while a markedly more disordered surface layer and shorter residence times are observed in MD simulations for the butyl halides as compared to the alcohol. Desorption from the interface was found to be less frequent for the butyl halides than for the methyl halides by MD simulations. Although Raman studies show uptake of the butyl alcohol into the bulk phase, neither Raman studies nor MD simulations provide any evidence for uptake of the butyl halides into the bulk phase. The profound difference in preferred orientations between alkyl halides and alcohols at the aqueous surface, with the halogen atom of the alkyl halides being to a large degree exposed to the vapor phase, is likely to have consequences for chemistry of alkyl halides adsorbed on the surface of atmospheric aerosol particles.

Introduction

Halogenated organic compounds of both biogenic and anthropogenic origin are abundant in the atmosphere and have been recognized to play important roles in both tropospheric and stratospheric chemistry.[1] Of the alkyl halides, methyl chloride (CH_3Cl) is of particular interest because it is the largest contributor of organic chlorine to the atmosphere[2,3] with an average tropospheric mixing ratio of approximately 540 pptv.[4,5] A significant fraction of the CH_3Cl present in the atmosphere is biogenic in origin,[4,5] and a great deal of research in recent years has been focused on balancing the global CH_3Cl budget because the known sinks of CH_3Cl outweigh the known sources.[3,4,6] The primary sources of CH_3Cl that are currently known include biomass burning,[7] wood-rot fungi,[8] tropical coastal land,[9] various tropical plants,[10] coastal salt marshes,[11,12] and the ocean,[4,13] which also serves as a net sink of CH_3Cl at high latitudes.[13,14] In the troposphere, the primary sink of CH_3Cl is reaction with OH radical.[4] However, the relatively long tropospheric lifetime of CH_3Cl (> 1 year) results in a significant amount of CH_3Cl being transported into the stratosphere, where it undergoes photolysis to release ozone-destroying Cl atoms.[3,15]

Halogens have also been implicated in the destruction of ozone in the troposphere. For several years, surface-level ozone depletion events have been observed in the Arctic at polar sunrise and have been correlated to an increase in gas-phase Br atom concentration, suggesting that atomic Br is an important component in the ozone destruction cycle.[16−20] However, the mechanisms for production of Br atom and its precursors have not been fully elucidated, nor have the chemical identities of the precursors been determined with great certainty.[21] One of the first mechanisms proposed for initiation of the ozone depletion event was photolysis of gas-phase bromoform.[17] Although it has subsequently been suggested that this pathway is not significant enough to account for the degree of ozone destruction,[22] the possible role of halogenated organic species, such as alkyl halides, in such processes must not be overlooked.

Alternatively, oxidation of halide ions in sea salt aerosol, the frozen ocean surface, and the Arctic snowpack has been

† Part of the "Max Wolfsberg Festschrift".

* Corresponding authors. E-mail: allen@chemistry.ohio-state.edu; roesel@uochb.cas.cz.

‡ The Ohio State University.

§ University of South Bohemia.

|| Academy of Sciences of the Czech Republic.

10.1021/jp808630v CCC: $40.75
Published on Web 02/05/2009

postulated as a possible pathway to the formation of reactive Br species involved in the ozone depletion events.[23,24] Both bulk aqueous phase and heterogeneous reactions have been shown to be important in the postulated mechanisms.[21−27] Because the concentration of halide ions is enhanced at the surface of sea salt aerosols and in frost flowers on the frozen ocean surface as compared to bulk-phase seawater,[28−31] interfacial processes leading to the activation of halides and other surface species must be considered for other atmospheric processes as well.

The importance of heterogeneous atmospheric processes has been demonstrated previously.[1] For example, evidence exists for the formation of a surface complex ($OH\cdots Cl^-$) during the production of gas-phase molecular chlorine from interfacial aqueous Cl^- and gas-phase OH.[28] In this case, single-phase reactions alone were unable to account for the experimentally observed production of molecular chlorine, and inclusion of the interfacial processes was necessary to make the model predictions consistent with the experimental observations.

Without doubt, single-phase chemical reactions are extremely important in describing atmospheric processes. However, such reactions cannot adequately account for all of the chemistry in our atmosphere, and important heterogeneous reactions must also be taken into account. Considering that the known biogeochemical cycle of CH_3Cl involves partitioning between different phases, it is reasonable that alkyl halides might also participate in interfacial processes. Alkyl halide species have been observed in the Arctic, where the potential for interfacial chemistry on aerosols, the open ocean, the snowpack, and the quasi-liquid layer of ice is significant.[32]

Here, vibrational sum frequency generation (VSFG) spectroscopy is used to study the residence and surface organization of gas-phase CH_3Cl adsorbed onto the surface of water. In addition, Raman spectroscopy is used to study the uptake of CH_3Cl into the bulk aqueous phase. These experiments are performed as necessary first steps in understanding possible surface reactivity and multiphase partitioning of alkyl halides. The results obtained for CH_3Cl are compared to those obtained for methyl alcohol (CH_3OH), which is also present in the Arctic troposphere.[33] Recent field observations indicate that CH_3OH is taken up into the interstitial air of the porous snowpack, where the surface area of the snowpack in contact with air is substantial.[33] VSFG results of a longer-chain series, comprising *n*-butyl chloride, *n*-butyl bromide, and *n*-butyl alcohol, are also presented. The experimental techniques are complemented by molecular dynamics (MD) simulations of methyl chloride, methyl bromide, *n*-butyl chloride, and *n*-butyl bromide at the air/aqueous interface to obtain detailed, molecular level information about the adsorption and organization of gaseous alkyl halides on the liquid water surface. Control simulations for methyl alcohol and *n*-butyl alcohol were also carried out. The results of the MD simulations are used to get insight into the experiment and aid the interpretation of the acquired experimental data.

Experimental Section

VSFG Theory. Detailed theoretical descriptions of the sum frequency process are available in the literature.[34−39] Only a brief description of this technique is presented here. VSFG is a second-order nonlinear optical technique that provides vibrational spectra of interfacial molecules. In VSFG, the sum frequency beam is generated by spatially and temporally overlapping a visible beam with an infrared beam at a sample surface. The resulting sum frequency beam has a frequency, ω_{SFG}, that is the sum of the frequencies of the two incident beams, ω_{VIS} and ω_{IR}, as shown in eq 1.

$$\omega_{SFG} = \omega_{VIS} + \omega_{IR} \tag{1}$$

The detected sum frequency signal originates from the molecules residing at the interface between two isotropic bulk phases and provides molecular-level structural information of these molecules. Polarization analysis of the sum frequency signal aids in spectral interpretation.

The intensity of the sum frequency signal is shown in eq 2.

$$I^{\omega_{SFG}}(\omega) \propto |E^{\omega_{SFG}} \cdot \chi^{(2)} : E^{\omega_{VIS}} E^{\omega_{IR}}|^2 I^{\omega_{VIS}} I^{\omega_{IR}} \tag{2}$$

$I^{\omega_{SFG}}$, $I^{\omega_{VIS}}$, and $I^{\omega_{IR}}$ are the intensities of the sum frequency, incident visible, and incident infrared beams, respectively. $\chi^{(2)}$ is the macroscopic second-order nonlinear susceptibility tensor for the interfacial molecules, and the absolute square term is the electric field at the interface, where the indicated *E* terms include Fresnel factors that describe the relationship between the induced nonlinear polarization of the interface and both the incoming beams and the generated sum frequency beam. Detailed mathematical representations of the Fresnel factors can be found in the literature.[36,39−41]

$\chi^{(2)}$ is comprised of a nonresonant term and a sum of resonant terms, as shown in eq 3.

$$|\chi^{(2)}|^2 = |\chi^{(2)}_{NR} + \sum_v \chi^{(2)}_v|^2 \tag{3}$$

$\chi^{(2)}_v$, the macroscopic nonlinear susceptibility for a vibration v, is related to the molecular hyperpolarizability for that vibration, as shown in eq 4.

$$\chi^{(2)}_v = N \sum_{lmn} \langle \mu_{IJK:lmn} \rangle \beta_v \tag{4}$$

N represents the number density of the surface species; β_v represents the molecular hyperpolarizability for the v vibrational mode; $\mu_{IJK:lmn}$ represents an Euler angle transformation between the laboratory reference frame (denoted by subscripts *I*, *J*, and *K*) and the molecular reference frame (denoted by subscripts *l*, *m*, and *n*); and $\langle\cdots\rangle$ represents an average over the orientational distribution of the molecules. The representation of the molecular hyperpolarizability in the molecular reference frame is shown in eq 5.

$$\beta_{lmn,v} = \frac{\langle g|\alpha_{lm}|v\rangle \langle v|\mu_n|g\rangle}{\omega_{IR} - \omega_v + i\Gamma_v} \tag{5}$$

ω_v is the frequency of the vibrational transition; Γ is the natural line-width of the transition; $\langle g|\alpha_{lm}|v\rangle$ is the Raman transition moment; and $\langle v|\mu_n|g\rangle$ is the infrared transition moment, where g is the ground vibrational state and v is the excited vibrational state. When the frequency of the incident infrared beam approaches the frequency of the vibrational transition, $\omega_{IR} - \omega_v$ approaches zero and the value of $\chi^{(2)}_v$ increases, resulting in an increase in the intensity of the sum frequency signal. Furthermore, the molecular hyperpolarizability is nonzero only when the Raman and infrared transition moments are nonzero. Thus, a vibrational mode must be both Raman and infrared active for it to be sum frequency active. Symmetry constraints arising from this selection rule lead to the requirement for a lack of inversion symmetry for sum frequency generation to be allowed. Macroscopically, this requirement is fulfilled at interfaces between two isotropic bulk phases. Sum frequency generation is forbidden in bulk phases where the molecules experience a centrosymmetric environment. The molecules residing at the interface between two isotropic bulk phases

experience a noncentrosymmetric environment and are sum frequency active by this selection rule. Furthermore, a bilayer exhibiting perfect inversion symmetry would be sum frequency inactive, whereas sum frequency signal would result from a monolayer or trilayer.

VSFG Instrumentation. The broad bandwidth sum frequency generation (BBSFG) spectrometer[42,43] employed in these experiments uses two regenerative amplifiers (Spectra-Physics Spitfire, femtosecond and picosecond versions) to produce femtosecond and picosecond visible pulsed laser beams with 1 kHz repetition rates. Each regenerative amplifier is seeded by one-half of the output from a mode-locked Ti:Sapphire laser (Spectra-Physics Tsunami) and is pumped by a Q-switched all solid-state Nd:YLF laser (Spectra-Physics Evolution-30). The output of the femtosecond regenerative amplifier (800 nm center wavelength, ~300 cm^{-1} bandwidth, 85 fs pulse duration)[42] is used in an optical parametric amplifier (OPA, Spectra-Physics OPA-800CF) to generate broad bandwidth infrared pulses (>300 cm^{-1} in the C−H stretching region). The wavelength region of the infrared output is selected by angle tuning a β-barium borate crystal in the OPA. The broad bandwidth infrared beam is spatially and temporally overlapped at the sample surface with the output of the picosecond regenerative amplifier (800 nm center wavelength, 15 cm^{-1} bandwidth, 2 ps pulse duration)[42] to generate the broad bandwidth sum frequency beam. A copropagating geometry is used for the visible and infrared beams, and the reflected sum frequency beam is detected. The angles of the infrared, visible, and sum frequency beams from the surface normal are 69°, 58°, and 60°, respectively.

The reflected visible beam is spatially filtered after the sample, and all residual light is optically filtered by two short pass (SPF-750, CVI, Albuquerque, NM) and two notch (Kaiser Optical Systems, Inc., Ann Arbor, MI) filters positioned in the sum frequency beam line. The sum frequency beam is dispersed by a 1200 g/mm grating blazed at 750 nm in a 500 mm monochromator (Acton Research, SpectraPro SP-500) and then detected by a liquid nitrogen-cooled CCD (Roper Scientific, LN 400EB, back-illuminated, 1340 × 400 pixel array). The monochromator is controlled using SpectraSense software (Acton Research, version 4.4.0).

Sum frequency peak positions are calibrated in the C−H stretching region using the absorption bands of a polystyrene film positioned in the infrared beam line during acquisition of a sum frequency spectrum of a GaAs crystal. Background spectra are acquired for each sample by disrupting the temporal overlap of the beams, and the background-subtracted sum frequency spectra are normalized to the nonresonant signal from a GaAs crystal surface. Polarization selection is achieved using a MgF_2 window in the infrared beam, a half-wave plate in the visible beam, and a Glan polarizer in the sum frequency beam. The resolution of the BBSFG system is approximately 8 cm^{-1}.[44]

Materials. Methyl alcohol (CH_3OH; HPLC grade), *n*-butyl chloride (C_4H_9Cl; ACS certified), and *n*-butyl alcohol (C_4H_9OH; ACS certified) were obtained from Fisher Scientific. *n*-Butyl bromide (C_4H_9Br; 99+% purity) was obtained from Acros Organics. Methyl chloride (CH_3Cl; 99.5% purity, instrument grade) was obtained from Scott Specialty Gases, Inc. (Plumsteadville, PA). Nitrogen (NF, compressed) was obtained from Praxair, Inc. (Danbury, CT). All chemicals were used as received. Deionized water was obtained from a Barnstead Nanopure filtration system with a minimum resistivity of 18.2 MΩ cm.

Experimental Method. To monitor the adsorption of gas-phase alcohols and alkyl halides to the aqueous surface, a flow chamber was used in combination with the BBSFG system. The flow chamber was attached to the sample stage of the BBSFG system, and the gas-phase species of interest was flowed over 24 mL of water in a Petri dish contained in the chamber while continuous VSFG spectra (60 s acquisitions) were obtained for up to 2 h. Approximately 6.5 μJ of infrared energy and 300 μJ of visible energy were used for these experiments, and all spectra shown were acquired in the SSP polarization combination. PPP and SPS spectra were also acquired and are shown in the Supporting Information. Background spectra were obtained for each sample throughout each flow experiment by disrupting the temporal overlap of the incident beams. All VSFG spectra are background-subtracted and normalized to the nonresonant VSFG signal from a GaAs crystal. The effect of evaporation was tested during these experiments to ensure proper overlap of the incident pulses.

The chamber used for the adsorption experiments is comprised of a stainless steel lid that attaches to a stainless steel cylindrical base by using knife-edge sealing technology in conjunction with a copper gasket (4 in. i.d.). The incident beams enter the chamber through a BaF_2 viewport (Reflex Analytical Corp., p/n 8960-1BAF2) on the chamber lid, and the SFG beam exits the chamber through a BK7 viewport (Kurt J. Lesker Co., p/n VPZL-275BK7). Because the optical properties of the windows affect the spatial and temporal overlap of the incident beams inside the flow chamber (as compared to when the chamber lid is removed), the overlap of the beams was optimized while monitoring the VSFG signal from a sample of sodium dodecyl sulfate (SDS) inside the flow chamber before the adsorption experiments were performed. The base of the chamber was lined with Teflon tape to minimize scattering of light inside the chamber, and a Teflon ring was used around the Petri dish to hold the sample in place inside the chamber.

Volatilization of the liquid samples (CH_3OH, C_4H_9OH, C_4H_9Cl, and C_4H_9Br) was accomplished by flowing nitrogen gas at 15 standard cm^3/min (sccm) through the liquid of interest contained in a glass vial. A flow controller (MKS Instruments, model 1479A51CS1BM; used with control box model PR4000-F2V1N) was used to maintain a steady flow of nitrogen gas into the liquid sample. Teflon tubing (1/8 in. o.d.) and Swagelok fittings were used to connect the flow controller to a stainless steel needle that was inserted into the liquid sample through a rubber septum. The nitrogen gas was bubbled into the liquid sample, and the gas mixture (volatilized species and nitrogen gas) was transported out of the vial and into the flow chamber using a second needle attached to Teflon tubing (1/4 in. o.d.). The opening of the second needle was placed approximately 1 in. above the surface of the liquid sample. Swagelok fittings were used to attach the tubing to both the collection needle and an inlet port in the flow chamber lid.

Because CH_3Cl has a very high vapor pressure at room temperature, the liquid was contained in a nonpressurized tank. The methyl chloride vapor was extracted from the container using a low-pressure regulator (Scott Specialty Gases, Inc., model 051202A510). Teflon tubing (1/4 in. o.d.) connected the regulator to a flow controller that was operated at 10 sccm. The output of the flow controller was connected to the flow chamber using Teflon tubing (1/4 in. o.d.). The fluxes (number of molecules per minute) were calculated by the weight difference for the liquid samples, whereas for the methyl chloride the ideal gas equation was used. (Ideal behavior was assumed because the sample chamber was open to the atmosphere during methyl chloride flow.) The fluxes were calculated to be 1.9×10^{20} and 2.5×10^{20} molecules/minute for methyl alcohol and methyl

chloride, respectively. Gas (as a function of time) and liquid concentrations are reported in the Supporting Information.

For all species, the experiments were performed at 24 °C and ambient pressure, and the vapor was exhausted from the flow chamber through an outlet on the lid. The organic vapors were purged from the cell using a flow of pure nitrogen gas after the adsorption experiments. The aqueous samples were then collected for subsequent bulk-phase analysis using a Raman spectrometer.

The Raman spectrometer employed in these experiments uses a 532 nm continuous wave laser (Process Instruments; model PI-ECL-785-300-SH) as an excitation source. The laser beam (0.2 mW) is delivered to the sample by the same fiber optic probe (InPhotonics) used to collect the scattered light. The scattered light is dispersed by a 600 g/mm grating blazed at 1 μm in a 500 mm monochromator (Acton Research, SpectraPro 500i; 50 μm slit width) and detected using a liquid nitrogen-cooled CCD (Roper Scientific, LN 400EB, back-illuminated, deep depletion, 1340 × 400 pixel array). The monochromator is controlled using SpectraSense software (Acton Research, version 4.2.9) and calibrated to the 435.83 nm line of fluorescent light. The peak positions of the Raman spectra are calibrated by comparing the position of experimentally observed naphthalene peaks to those in the literature.[45] An acquisition time of 3 min was used for the Raman experiments. All reported peak frequencies (for both Raman and VSFG spectra) are the observed frequencies, not from spectral fits.

MD Simulations. Molecular dynamics simulations of the adsorption of alkyl halides to the aqueous surface were performed using a water slab with two independent liquid/vapor interfaces. The simulation box contained 864 water molecules. The size of the box was set to 30 Å × 30 Å × 100 Å, with the elongated box dimension along the *z*-axis normal to the two liquid/vapor interfaces. An interface is defined as the region between 90% and 10% of the bulk water density. Periodic boundary conditions were applied in all three dimensions. Following a 250 ps equilibration of the water slab at 298 K, selected alkyl halide molecules (CH_3Cl, CH_3Br, C_4H_9Cl, or C_4H_9Br) were added into the simulation box. Simulations were carried out for 2 and for 50 alkyl halide molecules in the unit cell. Initial configurations for the trajectories were obtained by placing one-half of the total number of the alkyl halide molecules (i.e., 1 or 25) into the gas-phase region of the simulation box approximately 2 Å away from each of the two interfaces. The 25 alkyl halide molecules were initially placed on a regular grid in the *xy* plane. All systems were first energy minimized to avoid bad contacts, and subsequently equilibrated for several hundreds of picoseconds before a 10 ns production run. Control simulations for corresponding alcohols (CH_3OH and C_4H_9OH) were also carried out. All simulations were performed with a time step of 1 fs at a constant volume and a constant temperature of 298 K. Atomic coordinates were saved for further analysis every 500 steps (=0.5 ps). The nonbonded interactions were cut off at 12 Å, and long-range electrostatic interactions were accounted for using the Particle Mesh Ewald procedure.[46] All bonds involving hydrogen atoms were constrained using the SHAKE algorithm.[47] A polarizable force field was employed in all MD simulations. For water, we used the POL3 model.[48] For alkyl halides and methanol, the general Amber force field (GAFF) parameter set[49] was employed. Atomic partial charges for the alkyl halide molecules were evaluated using the standard RESP procedure employing the Gaussian 03 package.[50] The force field for butanol was adopted from Krisch et al.[51] All molecular dynamics calculations were performed using the Amber 8 program.[52]

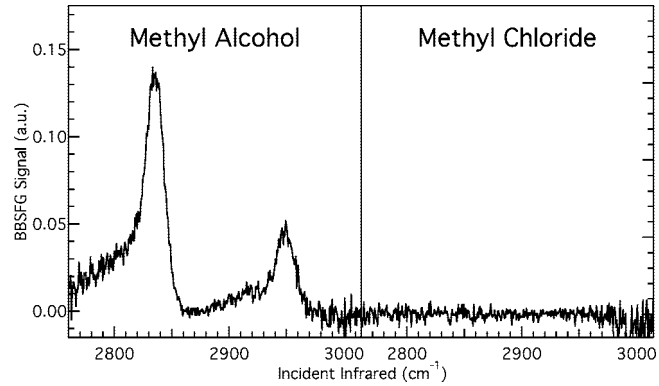

Figure 1. VSFG spectra from flow experiments over water: methyl alcohol (left panel) and methyl chloride (right panel) adsorbed to the aqueous surface.

Results and Discussion

Methyl Alcohol, Methyl Chloride, and Methyl Bromide at the Air/Water Interface. ***Spectroscopy, Methyl Species.*** The VSFG spectra obtained after 2 h of flow of CH_3OH (left panel) and CH_3Cl (right panel) over an aqueous surface are shown in Figure 1. In the spectrum of adsorbed CH_3OH, the peak at 2835 cm^{-1} is assigned to the CH_3 symmetric stretch (SS) and the peak at 2948 cm^{-1} is assigned to a CH_3 Fermi resonance (FR) with the shoulder at 2912 cm^{-1} assigned to a second CH_3 FR.[43] The VSFG peak intensities of methyl alcohol increase over time (Supporting Information, Figure S4), showing that this system does not come to equilibrium. Because sum frequency intensity is a function of both number density and orientational order, the presence of peaks in the VSFG spectrum of CH_3OH at the water surface suggests that the adsorbed CH_3OH molecules are not completely disordered at the air−aqueous interface, but rather have a preferential orientation at the interface. Previous MD studies of short chain alcohols at the air/aqueous interface indicate that the hydroxyl group of the alcohol hydrogen bonds to the surface water molecules.[53−57] This suggests that the preferential orientation of short chain alcohols at the air/aqueous interface is such that the hydrophilic hydroxyl group associates with the aqueous phase, and the hydrophobic alkyl group points into the gas phase. Thus, the CH_3OH molecules adsorbed at the air/aqueous interface adopt an organized surface structure.

In comparison, no peaks are observed in the VSFG spectrum of CH_3Cl at the air/aqueous interface, indicating that CH_3Cl either does not adsorb to the aqueous surface upon collision or does adsorb to the aqueous surface, but has a low number density, disordered interfacial arrangement, very short surface residence time, or some combination of these phenomena. From our gas-phase measurements, it is observed that the methyl chloride system has reached a steady state condition (Supporting Information, Figure S3). Understanding the possible uptake of CH_3Cl molecules from the gas phase into the bulk aqueous phase can aid in understanding the adsorption of CH_3Cl to the aqueous surface.

To determine whether CH_3Cl is taken up into the bulk liquid phase from the gas phase, the Raman spectrum of the bulk sample was obtained after the flow experiment and is shown in Figure 2 (red spectrum). A peak at 710 cm^{-1} is observed in the Raman spectrum of the aqueous CH_3Cl sample and is assigned to the C−Cl stretch of CH_3Cl.[58] The presence of a peak attributed to CH_3Cl in the spectrum of the bulk aqueous phase

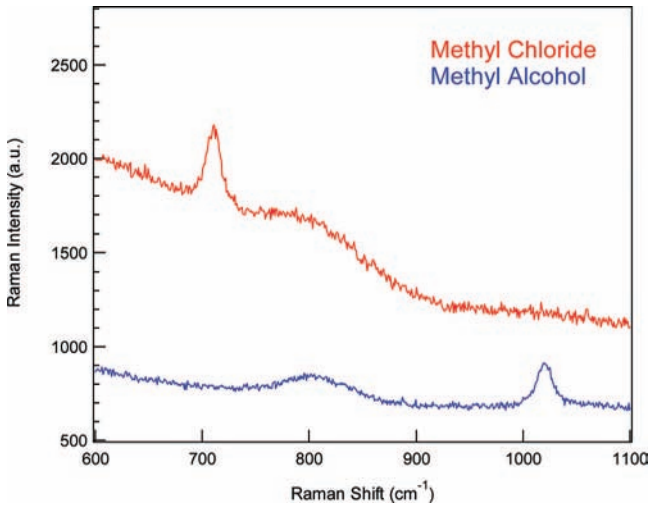

Figure 2. Raman spectra of bulk aqueous phase after flow experiments: C−Cl mode of methyl chloride (red, upper spectrum) and C−O mode of methyl alcohol (blue, lower spectrum).

is direct evidence that CH_3Cl is taken up into the aqueous phase from the gas phase during the flow experiments. In addition, the Raman spectrum of the CH_3OH bulk aqueous sample was obtained after the flow experiment and is shown in Figure 2 (blue spectrum). A peak at ∼1026 cm^{-1} is observed and assigned to the C−O symmetric stretching of CH_3OH. Uptake of gas-phase CH_3OH into the bulk aqueous phase has been reported previously.[59]

Although CH_3Cl is not detected at the interface during the VSFG experiments (within the detection limits of the BBSFG system under the experimental conditions used), the Raman bulk-phase studies indicate that some interaction of the gas-phase molecules with the aqueous interface must occur because uptake of CH_3Cl from the gas phase into the aqueous phase is observed (as is evident in Figure 2). To explain these results, a convolution of orientation and number density must be considered because the SFG intensity is proportional to these parameters as shown in eqs 2 and 4. Absorption of the incident infrared beam by the gas-phase molecules was considered, and although this was observed, more absorption from methyl alcohol than methyl chloride, the remaining infrared was sufficient to generate SFG from the methyl alcohol surface (details in Supporting Information).

By a simple comparison of electronegativities, the C−Cl bond in CH_3Cl is expected to be slightly more polar than the C−H bonds. Based on this model, the C−Cl bond might preferentially associate with the aqueous phase as compared to the more hydrophobic C−H bonds, which would then be expected to be oriented more toward the vapor phase. Orientational order with preference to lie perpendicular to the plane of the surface has been observed for CH_3Cl adsorbed to a layer of D_2O ice preadsorbed on Pd(111).[60]

Several possibilities can lead to a low number density of interfacial CH_3Cl molecules, including a low probability of adsorption upon collision, fast desorption from the surface for those molecules that do adsorb upon collision, or fast solvation of adsorbed molecules (i.e., fast uptake of adsorbed molecules into the bulk phase). The last two of these possibilities would lead to a short residence time of adsorbed CH_3Cl molecules.

Molecular Dynamics, Methyl Species. To examine surface number density, orientation, and interfacial residence times of methyl halides on the surface of liquid water, MD simulations were performed on systems containing 864 water molecules in

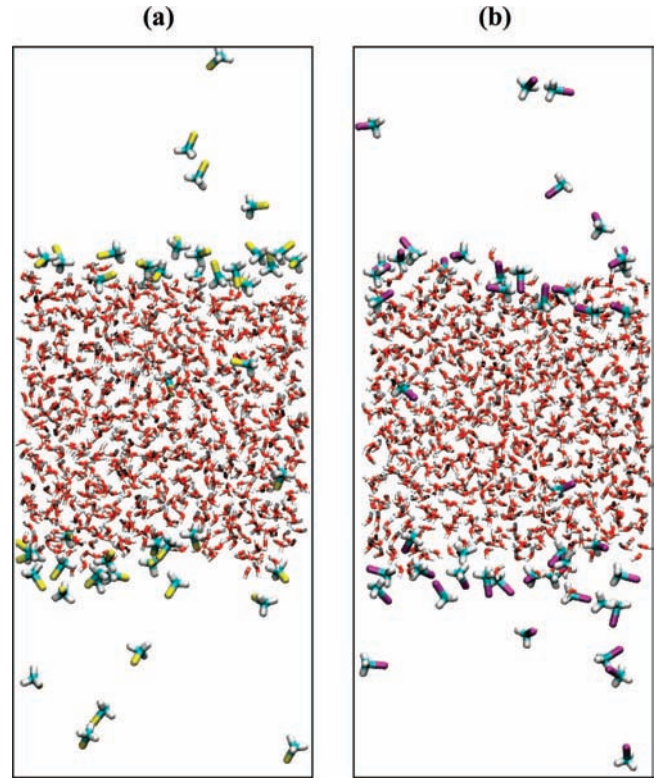

Figure 3. Snapshots from simulations of (a) 50 methyl chloride molecules and (b) 50 methyl bromide molecules and 864 water molecules in slab geometry. Color coding: red, oxygen; cyan, carbon; gray, hydrogen; magenta, bromine; yellow, chlorine.

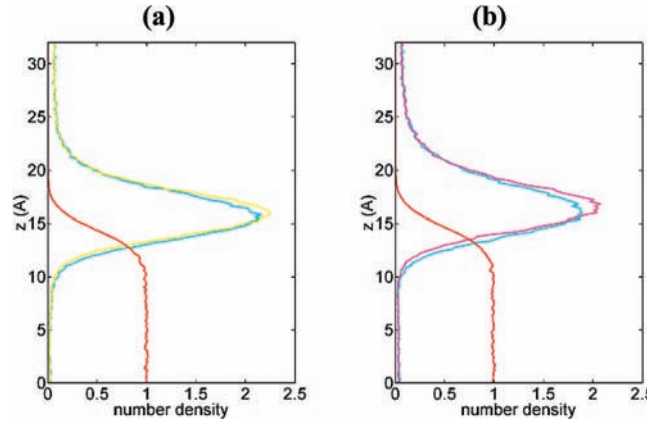

Figure 4. Density profiles resulting from simulations of (a) 50 methyl chloride molecules and (b) 50 methyl bromide molecules and 864 water molecules in slab geometry. Density profiles were averaged over the two equivalent interfaces. Color coding: red, oxygen; cyan, carbon; magenta, bromine; yellow, chlorine.

slab geometry and a total of 50 methyl chloride or methyl bromide molecules. The initial configuration consisted of 25 methyl halide molecules per each interface. Typical snapshots of the two systems are presented in Figure 3 with the corresponding density profiles shown in Figure 4. These figures clearly show that both methyl halides are present at the air/water interface, for their concentration is significantly enhanced in the interfacial region (defined on the z-axis as the interval in which the water density decreases from 90% to 10% of its value in the bulk liquid) as compared to the gas as well as the bulk liquid phase. During the simulation, individual CH_3Cl or CH_3Br molecules were observed to enter the interior of the water slab. However, entering the bulk is a rather rare event on the

nanosecond time scale of the simulation, fully in accord with the relatively low solubility and Henry's law constants of methyl halides (solubilities for the gas at a partial pressure of 1 atm in equilibrium with the solution,[61] CH_3Cl 5.35 g/L, CH_3Br 18.3 g/L; Henry's law constants,[62] CH_3Cl 0.10−0.13 mol atm^{-1}, CH_3Br 0.15−0.19 mol atm^{-1}). The CH_3Br molecules were observed to enter the bulk somewhat more readily and remained fully solvated for slightly longer times as compared to the CH_3Cl molecules. This is reflected in a slightly higher density profile signal of CH_3Br in the bulk region of the water slab with respect to CH_3Cl and is in agreement with somewhat higher solubility and Henry's law constant of CH_3Br over CH_3Cl. Throughout the simulation, the majority of the CH_3Cl and CH_3Br molecules remain located at the interface, although their interaction with the water surface is rather weak and there is frequent exchange of individual CH_3Cl or CH_3Br molecules between the interface and gas phase. This is in sharp contrast to methanol, which is very soluble in water and exhibits a surfactant activity at the aqueous interface.[53]

An interesting aspect of the density profiles depicted in Figure 4 is the fact that for both CH_3Cl and CH_3Br the surface peak of the carbon atom is shifted toward the interior of the water slab as compared to the halogen atom peak. This indicates that on average the methyl halide molecules are oriented with the CH_3 group, rather than the halogen atom, toward the water. This is a surprising finding because the analogy between methyl halides and methyl alcohol would seem to suggest that the geometry adopted by CH_3OH at the aqueous surface, in which the more hydrophilic OH moiety associates with the aqueous phase and the more hydrophobic CH_3 group points away from the aqueous surface,[53] is also likely to be adopted by methyl halide molecules adsorbed at the aqueous surface.

To verify that the orientation of the methyl halide molecules at the water surface predicted by the simulation is not an artifact of the model, for example, due to the CH_3Cl−CH_3Cl or CH_3Br−CH_3Br interactions at the interface, we performed another simulation in which only 2 CH_3Cl or CH_3Br molecules were introduced into the simulation box containing 864 water molecules in a slab geometry. The trajectories were initiated with one methyl halide molecule on each surface of the slab. In the course of the simulation, both molecules were occasionally present on the same interface, however, rarely in the vicinity of each other. As an example, trajectories of two CH_3Cl molecules are shown in Figure 5 as a plot of the z-coordinate of the Cl atom of CH_3Cl versus time. While the CH_3Cl molecules occasionally diffuse into the bulk liquid region of the slab, they mostly remain confined to the interfacial region, undergoing frequent desorption into the gas phase. Residence times of CH_3Cl molecules at the aqueous interface, observed in the simulation, range from a few picoseconds to ~1 ns, with a mean value of 140 ps. The trajectories of CH_3Br yielded essentially the same picture as for CH_3Cl and are therefore not shown here. In an analogous simulation for methyl alcohol, gaseous CH_3OH molecules were observed to adsorb to the water surface and, subsequently, diffuse into the interior of the aqueous slab, consistent with their large water solubility. In the course of the simulation, the solvated CH_3OH molecules revisited the interfacial region; however, desorption of methanol from the water surface back into the gas phase did not occur throughout the entire 10 ns trajectory.

The simulations of 2 CH_3Cl or CH_3Br molecules interacting with the water slab provided density profiles similar to the ones presented in Figure 4, confirming the results of the trajectories with 50 CH_3Cl or CH_3Br molecules in the simulation box, in particular with respect to the shift between the carbon and the halogen atom density profile peaks.

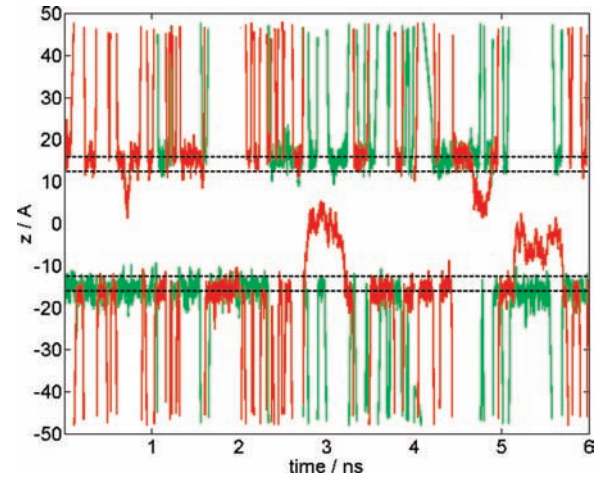

Figure 5. Trajectories of two methyl chloride molecules (one depicted in red, the other one in green) interacting with water slab. The two air/water interfaces of the water slab, defined as the regions between 10% and 90% of the liquid water density, are indicated by the dashed horizontal lines; $z = 0$ corresponds to the middle of the slab.

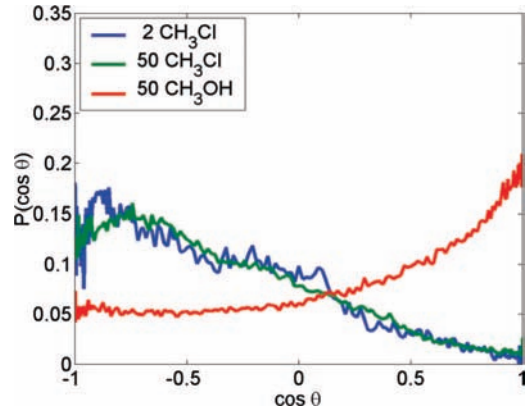

Figure 6. Orientation distribution of CH_3Cl and CH_3OH molecules at the air/water interface. Angle θ is defined as the angle between the interface normal and molecular axis (Cl → C vector for CH_3Cl and O → C vector for CH_3OH). Color coding: blue, 2 CH_3Cl molecules; green, 50 CH_3Cl molecules; red, 50 CH_3OH molecules in the simulation box.

The difference in preferred orientation between the methyl halide molecules and methanol is clearly visualized in Figure 6, which shows the orientation probability distributions for the CH_3Cl and CH_3OH molecules at the water/vapor interface as a function of $\cos(\theta)$, θ being the angle between the molecular axis (Cl → C vector in the case of CH_3Cl, O → C vector in the case of CH_3OH) and the vector normal to the air/aqueous interface. Thus, $\cos(\theta) = 0$ corresponds to the CH_3Cl or CH_3OH molecule oriented with the molecular axis parallel to the air/water interface, whereas $\cos(\theta) = \pm 1$ corresponds to the CH_3Cl or CH_3OH molecule oriented with the molecular axis along the interface normal; for $\cos(\theta) = 1$ pointing with the methyl group toward the gas phase, and for $\cos(\theta) = -1$ pointing with the methyl group toward water. Simulations with the higher dose of methyl halides (50 CH_3Cl) and with isolated methyl halide molecules (2 CH_3Cl) on the water surface yielded essentially identical probability distributions, with the lowest probability for $0.5 < \cos(\theta) < 1$, which corresponds to the CH_3Cl molecule pointing with the halide atom toward the interior of the water slab and the CH_3 group toward the vapor phase, and the

maximum probability within the interval $-1 < \cos(\theta) < -0.5$, which corresponds to the CH_3Cl molecule pointing with the halide atom toward the vapor phase and the CH_3 group toward the interior of the water slab. Thus, the CH_3 group of those CH_3Cl molecules that align along the surface normal will be more likely to interact with water than to stick out freely into the vapor phase. However, the distributions are rather broad, indicating a fairly high degree of orientational disorder and a presence of a considerable fraction of the molecules that are aligned parallel with the surface. For comparison, orientational distribution of 50 CH_3OH molecules from the simulation of methanol/water mixture is also shown. It exhibits a maximum for $\cos(\theta) = 1$, which corresponds to the preferred orientation of methanol at the interface with the methyl group pointing into the vapor phase.

The above results of MD simulations clearly indicate that, despite analogies in physical and chemical properties between alkyl halides and alcohols, methyl chloride and methyl bromide interact with the aqueous surface in a different way and adopt a different geometry at the air/water interface than methyl alcohol. Previous ab initio calculations[63,64] on CH_3Cl and CH_3Br and their complexes with water also show profound differences between these molecules and CH_3OH. While both CH_3OH and methyl halides are polar molecules (the dipole moment of CH_3OH is 1.61 debye, the dipole moments of CH_3Cl and CH_3Br are 1.97 and 1.93 debye, respectively[65]), the charge distribution in the CH_3OH molecule has a character rather different from that in the methyl halide molecules. The dipole moment of CH_3OH is oriented predominantly along the O−H bond, resulting in the methanol molecule consisting of a polar (OH) part and a nonpolar (CH_3) part, whereas methyl halides do not exhibit this amphiphilic character, having the dipole moment oriented along the molecular (C−Cl) axis. In addition, while the CH_3OH molecule can, through its OH group, engage in hydrogen bonding patterns both as an H-bond donor and an H-bond acceptor, the Cl or Br atom of the methyl halide molecule can only act as an H-bond acceptor.

These differences strongly affect the way in which methyl alcohol and methyl halides interact with water. In methyl alcohol, the hydroxyl group associates with the water molecules in clusters[66] as well as at the aqueous surface,[53] while the methyl group is oriented away from water, toward the gas phase. The character of bonding between methyl halides and water is quite different: the $CH_3X{:}H_2O$ and $CH_3X{:}(H_2O)_2$ complexes (X = Cl, Br) reported in the literature[63,64] were found to have a cyclic structure with a water hydrogen bonded to the halogen atom of the CH_3X moiety and one of the hydrogen atoms of the CH_3 group weakly bonded to water oxygen. The structure of the methyl halide−water complexes was correctly reproduced by our force field. At an aqueous surface, this bonding pattern is consistent with the halogen atom of CH_3X binding to a dangling hydrogen atom that is present at the air/water interface, while one or several of the H atoms of the CH_3 group weakly bind to the oxygen atoms of nearby water molecules. However, this simple static picture cannot capture all of the complexity of the (relatively weak) interaction between a methyl halide molecule and the surface of liquid water, which at ambient temperature continually undergoes reorganization at a picosecond time scale. Thus, the majority of structures sampled by the methyl halide molecule at the aqueous interface correspond to a nonamphiphilic polar molecule interacting with the surface of polar solvent.

In summary, the MD simulations show that gas-phase CH_3Cl and CH_3Br molecules do adsorb to the aqueous surface upon collision with essentially unit probability at room temperature. They do, in fact, accumulate at the interface if available at large enough number density in the gas phase above the aqueous interface, and they exhibit preference for (partial) solvation on the surface rather than full solvation in the bulk liquid. However, uptake of both CH_3Cl and CH_3Br into the interior of the water slab has been observed in the MD trajectories, which is consistent with the experimental observation of CH_3Cl in the bulk liquid phase using Raman spectroscopy. To explain the absence of the CH_3Cl signal in the VSFG spectrum, the combination of orientation disorder and low number density has been invoked. The MD simulations clearly show that the level of surface orientation disorder of both CH_3Cl and CH_3Br on water is much higher than for methyl alcohol, resulting in a smaller degree of net orientation of methyl halides at the aqueous interface. At the same time, while accumulation of methyl halide molecules at the air/water interface has been observed in the simulation with a high dose of methyl halide species, a low number density of interfacial CH_3Cl under the experimental conditions cannot be ruled out, given the short residence time obtained from MD simulation. The MD results indicate that the possible low interfacial number density is likely due to the short residence time of the adsorbed CH_3Cl molecules with respect to desorption from the surface back into the gas phase rather than with respect to absorption into the bulk liquid.

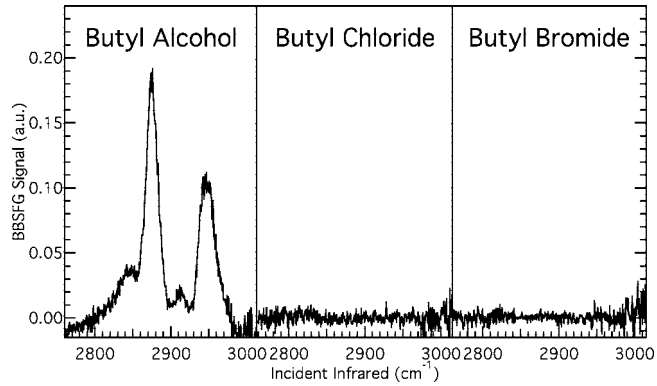

Figure 7. VSFG spectra from flow experiments over water: butyl alcohol (left panel), butyl chloride (center panel), and butyl bromide (right panel) adsorbed to the aqueous surface.

Butyl Alcohol, Butyl Chloride, and Butyl Bromide at the Air/Water Interface. ***Spectroscopy, Butyl Species.*** Comparison of the VSFG and Raman data for CH_3Cl and CH_3OH (presented in Figures 1 and 2) with complementary studies of water-insoluble species might help to elucidate the mechanisms of adsorption and uptake for the halide and alcohol species. The VSFG studies were performed on the butyl species, and the results are presented here. Both C_4H_9Cl and C_4H_9Br are insoluble in water, while butyl alcohol has a solubility of 115 g/L.[67]

VSFG spectra of the flow experiments using the longer-chain series (butyl alcohol − left panel, C_4H_9Cl − center panel, and C_4H_9Br − right panel) are shown in Figure 7. The same trend is observed for the butyl species as is observed for the methyl species. No VSFG intensity is observed for the halides, but peaks are observed in the VSFG spectrum for the alcohol. The peaks in the VSFG spectrum obtained for the flow experiment of butyl alcohol over water are assigned to the CH_2 SS (2845 cm^{-1}), CH_3 SS (2875 cm^{-1}), CH_2 FR (2911 cm^{-1}), and CH_3 FR (2945 cm^{-1}). These assignments are based on VSFG assignments for neat C_4H_9OH in the literature.[68] As with CH_3OH, the VSFG spectrum of C_4H_9OH at the water surface suggests that the

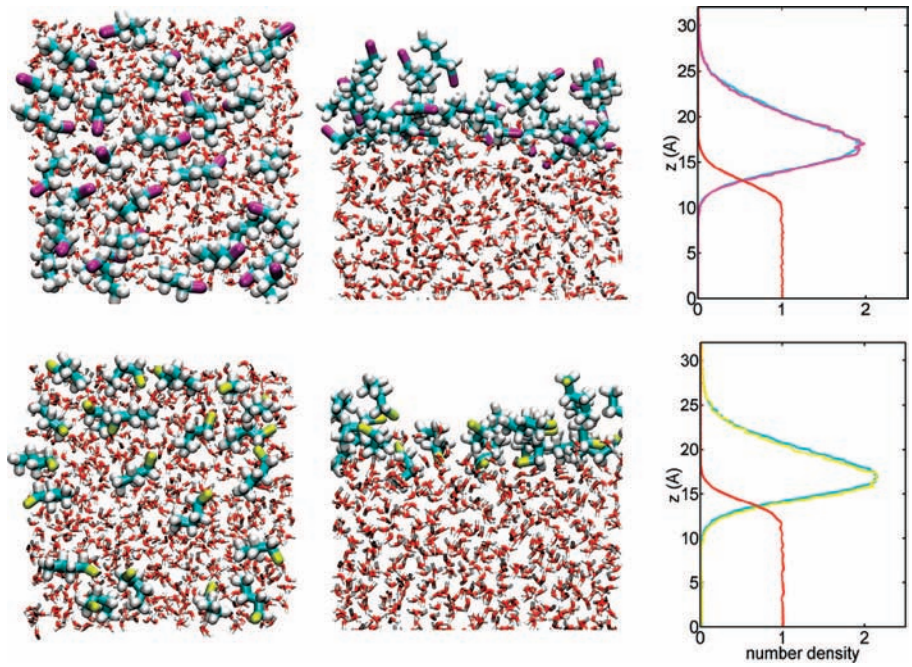

Figure 8. Representative snapshots (top view − left column, side view − middle column) and density profiles (right column) from simulations of 50 butyl halide molecules (approximately 25 per interface) with 864 water molecules in slab geometry (top row − butyl bromide, bottom row − butyl chloride). Density profiles were averaged over the two equivalent interfaces. Color coding: red, oxygen; cyan, carbon; gray, hydrogen; magenta, bromine; yellow, chlorine.

adsorbed C_4H_9OH molecules are not completely orientationally disordered at the interface. The presence of a peak corresponding to the CH_2 SS indicates that the adsorbed C_4H_9OH molecules possess some gauche defects. This finding is consistent with results reported in the literature.[51,68] Again, a convolution of orientation and number density prevents VSFG signal from being observed in the case of the butyl halide species. Raman spectra also revealed the presence of butyl alcohol in the bulk, although butyl halides were not detected (Supporting Information).

Molecular Dynamics, Butyl Species. To shed more light on the interaction of butyl chloride and butyl bromide molecules with the liquid water surface, molecular dynamics simulations were performed on systems consisting of 864 water molecules in slab geometry and 50 C_4H_9Cl or C_4H_9Br molecules (initially 25 per each liquid/vapor interface). During the simulation, the majority of the C_4H_9Cl as well as C_4H_9Br molecules remained adsorbed to the water surface. Occasionally, individual butyl halide molecules were observed to desorb into the gas phase, although desorption was less frequent than for methyl halides. No butyl halide molecule was observed to enter the bulk liquid region of the water slab for any significant amount of time, in accordance with negligible solubility of C_4H_9Cl and C_4H_9Br in water. The density profiles resulting from these simulations along with a snapshot of the C_4H_9Cl and C_4H_9Br molecules on one of the liquid water slab surfaces are presented in Figure 8.

While adsorbed at the air/water interface, butyl halides did not form a stable, well-ordered film. This finding is consistent with previous results reported in the literature.[69,70] As compared to butyl alcohol, which has been found to form a well-organized monolayer on the water surface, in which the OH groups interact with the aqueous phase and the hydrocarbon chains stand upright,[51,71] the surface-adsorbed layer of butyl halides exhibits a significantly larger degree of disorder.

To elucidate further the dynamics of butyl halide adsorption on the surface of liquid water, simulations of 2 C_4H_9Cl and C_4H_9Br molecules interacting with the water slab were performed. As an example, trajectories of two C_4H_9Br molecules (plotted as the z-coordinate of the Br atom vs time) are depicted in Figure 9. The results for C_4H_9Cl molecules are similar to C_4H_9Br and are therefore not shown here. As shown in Figure 9, butyl halide molecules adsorb to the water surface upon collision; however, they readily undergo desorption back into the gas phase, albeit somewhat less frequently as compared to methyl halide species. Surface residence times of C_4H_9Br molecules, observed in the simulation, range between several picoseconds and 3.3 ns, with a mean value of ~1 ns. This again is in stark contrast to butyl alcohol, which during analogous, 10 ns long simulation remains adsorbed at the water surface or diffuses throughout the interior of the aqueous slab.

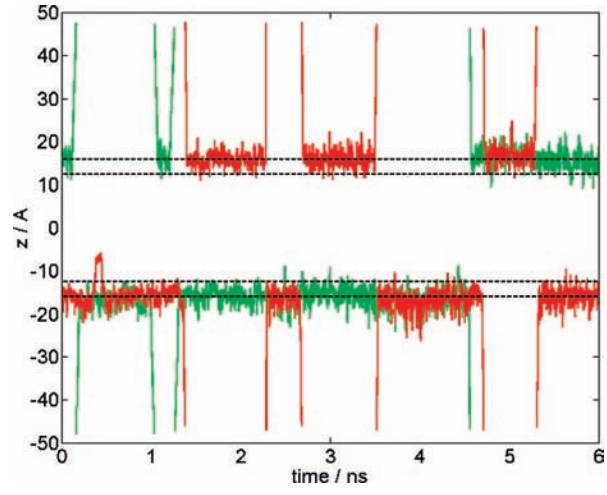

Figure 9. Trajectories of two butyl bromide molecules (one depicted in red, the other one in green) interacting with water slab. The two air/water interfaces of the slab, defined as the regions between 10% and 90% of the liquid water density, are indicated by the dashed horizontal lines; $z = 0$ corresponds to the middle of the slab.

To obtain more detailed information about the orientation of butyl halide molecules at the water/vapor interface, we performed

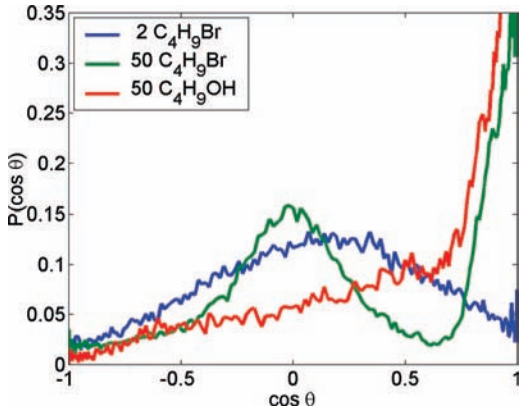

Figure 10. Orientation distribution of the terminal methyl groups of the C_4H_9Br and C_4H_9OH molecules at the air/water interface. Angle θ is defined as the angle between the vector normal to the interface and the C2 → C1 vector, where C1 is the terminal (methyl group) carbon atom. Color coding: blue, 2 C_4H_9Br molecules; green, 50 C_4H_9Br molecules; red, 50 C_4H_9OH molecules in the simulation box.

orientational analysis of two intramolecular vectors, u = C4 → C1 and v = C2 → C1, where C1 is the terminal (methyl group) carbon and C4 the carbon adjacent to the halogen atom of the butyl halide molecule, C_4H_9X (X = Cl, Br). The C4 → C1 vector was chosen to characterize the orientation of the hydrocarbon chain of the butyl halide molecules with respect to the interface, while the C2 → C1 vector was used to analyze the orientation of the terminal methyl group. The simulations of 2 alkyl halide molecules at the water surface yielded broad orientation distributions of the u = C4 → C1 vectors with a preference for the molecules to be aligned parallel to the surface. This finding is in agreement with the visual inspections of the trajectories in which a broad range of orientations was sampled by the (isolated) butyl halide molecules adsorbed at the aqueous interface; however, the hydrocarbon chains of the molecules were mostly found to lie flat on the water surface. In the case of 50 alkyl halide molecules in the simulation box, the C4 → C1 orientation distributions indicate an increase of the fraction of the butyl chloride and, in particular, butyl bromide molecules with the chains standing upright and the CH_3 group pointing into the gas phase. However, a significant fraction of molecules remain to be aligned parallel to the surface. These orientational characteristics of the butyl halide chains are reflected in the orientation distributions of the terminal methyl groups as depicted in Figure 10 for butyl bromide using the C2 → C1 vector (note that the C2 → C1 vector coincides with the c_3 symmetry axis of the CH_3 group). For the isolated butyl halide molecules, the C2 → C1 orientation distributions of the terminal methyl groups are rather broad with a preference for the axis of the CH_3 group to be aligned parallel to the surface ($\cos(\theta) = 0$). For the increased surface coverage, the maximum of the probability distributions shifts toward $\cos(\theta) = 1$, that is, the CH_3 group oriented upright, along the surface normal. A second maximum at $\cos(\theta) = 0$ corresponds to the fraction of molecules that remain oriented with the CH_3 group axis parallel to the surface. A control simulation of 50 butanol molecules in the simulation box confirmed the findings of previous studies,[51,71] that butanol molecules form a surface layer with alkyl chains standing upright and the OH group pointing toward the interface. In Figure 10, this behavior of the butanol molecules is reflected in the orientational distribution of their CH_3 end-groups, which exhibits the only maximum at $\cos(\theta) = 1$.

To summarize, MD simulations show that gas-phase C_4H_9Cl and C_4H_9Br molecules adsorb to the water surface. However, because their surface residence times with respect to desorption back into the gas-phase are quite short, large partial pressures are likely to be needed to achieve significant surface coverage. At the same time, it is only under the conditions of substantial surface coverage that a considerable fraction of chains align along the surface normal with the CH_3 group upright. In general, the surface adsorbed C_4H_9Cl and C_4H_9Br exhibit much larger orientation disorder than does the corresponding alcohol, C_4H_9OH. Thus, as in the case of CH_3Cl and CH_3Br, the results of the MD simulations indicate that both low number densities due to short residence times of butyl halides on the surface as well as the large degree of orientation disorder are likely to be the cause for the absence of the VSFG signal corresponding to C_4H_9Cl and C_4H_9Br.

Conclusions

Adsorption of gas-phase alkyl alcohols and alkyl halides to the air/water interface was studied using surface-sensitive vibrational sum frequency spectroscopy and molecular dynamic simulations. The alcohols studied here, methyl and butyl alcohol, adsorb at the air/aqueous interface and are then absorbed into the aqueous solution as revealed by surface (VSFG) and bulk (Raman) spectroscopies. The halides, methyl and butyl chloride, and butyl bromide, were not detected at the air/water interface, although methyl chloride was readily observed in the bulk. MD simulations reveal that the behavior of alkyl halides is significantly different relative to that of alkyl alcohols. Orientation and vapor/water residence times are considerably different. Consistent with the lack of signal from the VSFG spectra, MD simulations show that the alkyl halides are more disordered and have considerably shorter residence times relative to the alcohols at the air/water interface. The MD simulations also show that, quite surprisingly, surface-adsorbed methyl halides orient with the halogen atom exposed toward the vapor phase. The behavior of butyl halides on the water surface is somewhere between that of simple alkanes and alcohols (butyl halides predominantly align parallel to the surface, and, at larger coverage, a fraction of molecules has its hydrocarbon chain pointing into the vapor phase). These findings are likely to have consequences for atmospheric chemistry, in particular for photodissociation of methyl chloride and methyl bromide when adsorbed on an aerosol surface.

Acknowledgment. We acknowledge funding for this project from the National Science Foundation, NSF-ATM (# 0413893), and NSF-CHE (#0749807). The work in Prague was supported by the Czech Ministry of Education (grant LC512) and was performed within the framework of the research project Z40550506. Support to B.M. from the Institutional Research Concept of the Academy of Science of the Czech Republic (AVOZ60870520), from the Ministry of Education of the Czech Republic (LC 06010 and MSM6007665808), and the Grant Agency of the Czech Republic (203/08/0114) is also gratefully acknowledged. We wish to thank Pavel Jungwirth for stimulating discussions.

Supporting Information Available: VSFG spectra under PPP and SPS polarization combinations from flow experiments of CH_3OH, CH_3Cl, C_4H_9Cl, C_4H_9Br, and C_4H_9OH over water. Details of the concentration calculations of CH_3OH and CH_3Cl in the gas phase, and CH_3OH in the aqueous phase. Determination of the infrared energy during the flow of the gas-phase methyl species through the chamber. Raman spectra of the aqueous solutions after the flow of the butyl species. This material is available free of charge via the Internet at http://pubs.acs.org.

References and Notes

(1) Finlayson-Pitts, B. J.; Pitts, J. J. N. *Chemistry of the Upper and Lower Atmosphere*; Academic Press: New York, 2000.

(2) Graedel, T. E.; Keene, W. C. *Global Biogeochem. Cycles* **1995**, *9*, 47–77.
(3) Butler, J. H. *Nature (London)* **2000**, *403*, 260–261.
(4) Keene, W. C.; Khalil, M. A. K.; Erickson, D. J., III; McCulloch, A.; Graedel, T. E.; Lobert, J. M.; Aucott, M. L.; Gong, S. L.; Harper, D. B.; Kleiman, G.; Midgley, P.; Moore, R. M.; Seuzaret, C.; Sturges, W. T.; Benkovitz, C. M.; Koropalov, V.; Barrie, L. A.; Li, Y. F. *J. Geophys. Res., [Atmos.]* **1999**, *104*, 8429–8440.
(5) Khalil, M. A. K.; Moore, R. M.; Harper, D. B.; Lobert, J. M.; Erickson, D. J.; Koropalov, V.; Sturges, W. T.; Keene, W. C. *J. Geophys. Res., [Atmos.]* **1999**, *104*, 8333–8346.
(6) Yoshida, Y.; Wang, Y.; Zeng, T.; Yantosca, R. *J. Geophys. Res., [Atmos.]* **2004**, *109*, D24309/1–D24309/15.
(7) Lobert, J. M.; Keene, W. C.; Logan, J. A.; Yevich, R. *J. Geophys. Res., [Atmos.]* **1999**, *104*, 8373–8389.
(8) Watling, R.; Harper, D. B. *Mycol. Res.* **1998**, *102*, 769–787.
(9) Yokouchi, Y.; Noljiri, Y.; Barrle, L. A.; Toom-Sauntry, D.; Machlda, T.; Inuzuka, Y.; Aklmoto, H.; Li, H. J.; Fujinuma, Y.; Aoki, S. *Nature (London)* **2000**, *403*, 295–298.
(10) Yokouchi, Y.; Ikeda, M.; Inuzuka, Y.; Yukawa, T. *Nature (London)* **2002**, *416*, 163–165.
(11) Bill, M.; Rhew, R. C.; Weiss, R. F.; Goldstein, A. H. *Geophys. Res. Lett.* **2002**, *29*, 4/1–4/4.
(12) Rhew, R. C.; Miller, B. R.; Weiss, R. F. *Nature (London)* **2000**, *403*, 292–295.
(13) Rasmussen, R. A.; Rasmussen, L. E.; Khalil, M. A. K.; Dalluge, R. W. *J. Geophys. Res., [Oceans]* **1980**, *85*, 7350–7356.
(14) Moore, R. M.; Groszko, W.; Niven, S. J. *J. Geophys. Res., [Oceans]* **1996**, *101*, 28529–28538.
(15) Khalil, M. A. K.; Rasmussen, R. A. *Atmos. Environ.* **1999**, *33*, 1305–1321.
(16) Anlauf, K. G.; Mickle, R. E.; Trivett, N. B. A. *J. Geophys. Res., [Atmos.]* **1994**, *99*, 25345–25353.
(17) Barrie, L. A.; Bottenheim, J. W.; Schnell, R. C.; Crutzen, P. J.; Rasmussen, R. A. *Nature (London)* **1988**, *334*, 138–141.
(18) Bottenheim, J. W.; Gallant, A. G.; Brice, K. A. *Geophys. Res. Lett.* **1986**, *13*, 113–116.
(19) Oltmans, S. J.; Komhyr, W. D. *J. Geophys. Res., [Atmos.]* **1986**, *91*, 5229–5236.
(20) Tarasick, D. W.; Bottenheim, J. W. *Atmos. Chem. Phys.* **2002**, *2*, 197–205.
(21) Foster, K. L.; Plastridge, R. A.; Bottenheim, J. W.; Shepson, P. B.; Finlayson-Pitts, B. J.; Spicer, C. W. *Science* **2001**, *291*, 471–474.
(22) Finlayson-Pitts, B. J. *Chem. Rev.* **2003**, *103*, 4801–4822.
(23) Finlayson-Pitts, B. J.; Livingston, F. E.; Berko, H. N. *Nature (London)* **1990**, *343*, 622–625.
(24) Tang, T.; McConnell, J. C. *Geophys. Res. Lett.* **1996**, *23*, 2633–2636.
(25) Domine, F.; Shepson, P. B. *Science* **2002**, *297*, 1506–1510.
(26) Fan, S. M.; Jacob, D. J. *Nature (London)* **1992**, *359*, 522–524.
(27) Mozurkewich, M. *J. Geophys. Res., [Atmos.]* **1995**, *100*, 199–207.
(28) Knipping, E. M.; Lakin, M. J.; Foster, K. L.; Jungwirth, P.; Tobias, D. J.; Gerber, R. B.; Dabdub, D.; Finlayson-Pitts, B. J. *Science* **2000**, *288*, 301–306.
(29) Koop, T.; Kapilashrami, A.; Molina, L. T.; Molina, M. J. *J. Geophys. Res., [Atmos.]* **2000**, *105*, 26393–26402.
(30) Mucha, M.; Frigato, T.; Levering, L. M.; Allen, H. C.; Tobias, D. J.; Dang, L. X.; Jungwirth, P. *J. Phys. Chem. B* **2005**, *109*, 7617–7623.
(31) Rankin, A. M.; Auld, V.; Wolff, E. W. *Geophys. Res. Lett.* **2000**, *27*, 3469–3472.
(32) Swanson, A. L.; Blake, N. J.; Dibb, J. E.; Albert, M. R.; Blake, D. R.; Sherwood Rowland, F. *Atmos. Environ.* **2002**, *36*, 2671–2682.
(33) Boudries, H.; Bottenheim, J. W.; Guimbaud, C.; Grannas, A. M.; Shepson, P. B.; Houdier, S.; Perrier, S.; Domine, F. *Atmos. Environ.* **2002**, *36*, 2573–2583.
(34) Gopalakrishnan, S.; Jungwirth, P.; Tobias, D. J.; Allen, H. C. *J. Phys. Chem. B* **2005**, *109*, 8861–8872.
(35) Hirose, C.; Akamatsu, N.; Domen, K. *J. Chem. Phys.* **1992**, *96*, 997–1004.
(36) Lambert, A. G.; Davies, P. B.; Neivandt, D. J. *Appl. Spectrosc. Rev.* **2005**, *40*, 103–145.
(37) Moad, A. J.; Simpson, G. J. *J. Phys. Chem. B* **2004**, *108*, 3548–3562.
(38) Shen, Y. R. *The Principles of Nonlinear Optics*; Wiley: New York, 1984.
(39) Zhuang, X.; Miranda, P. B.; Kim, D.; Shen, Y. R. *Phys. Rev. B: Condens. Matter Mater. Phys.* **1999**, *59*, 12632–12640.
(40) Gopalakrishnan, S.; Liu, D.; Allen, H. C.; Kuo, M.; Shultz, M. J. *Chem. Rev.* **2006**, *106*, 1155–1175.
(41) Hirose, C.; Akamatsu, N.; Domen, K. *Appl. Spectrosc.* **1992**, *46*, 1051–1072.
(42) Hommel, E. L.; Ma, G.; Allen, H. C. *Anal. Sci.* **2001**, *17*, 1325–1329.
(43) Ma, G.; Allen, H. C. *J. Phys. Chem. B* **2003**, *107*, 6343–6349.
(44) Ma, G.; Allen, H. C. *Photochem. Photobiol.* **2006**, *82*, 1517–1529.
(45) McCreery, R. L. *Raman Spectroscopy for Chemical Analysis*; John Wiley & Sons: New York, 2000.
(46) Essman, U.; Perera, L.; Berkowitz, M. L.; Darden, T.; Lee, H.; Pedersen, L. G. *J. Chem. Phys.* **1995**, *103*, 8577–8593.
(47) Ryckaert, J.-P.; Ciccotti, G.; Berendsen, H. J. C. *J. Comput. Phys.* **1977**, *23*, 327–341.
(48) Caldwell, J. W.; Kollman, P. A. *J. Phys. Chem.* **1995**, *99*, 6208–6219.
(49) Wang, J. M.; Wolf, R. M.; Caldwell, J. M.; Kollman, P. A.; Case, D. A. *J. Comput. Chem.* **2004**, *25*, 1157–1174.
(50) Frisch, M. J. T. G. W.; Schlegel, H. B.; Scuseria, G. E.; Robb, M. A.; Cheeseman, J. R.; Montgomery, J. A., Jr.; Vreven, T.; Kudin, K. N.; Burant, J. C.; Millam, J. M.; Iyengar, S. S.; Tomasi, J.; Barone, V.; Mennucci, B.; Cossi, M.; Scalmani, G.; Rega, N.; Petersson, G. A.; Nakatsuji, H.; Hada, M.; Ehara, M.; Toyota, K.; Fukuda, R.; Hasegawa, J.; Ishida, M.; Nakajima, T.; Honda, Y.; Kitao, O.; Nakai, H.; Klene, M.; Li, X.; Knox, J. E.; Hratchian, H. P.; Cross, J. B.; Bakken, V.; Adamo, C.; Jaramillo, J.; Gomperts, R.; Stratmann, R. E.; Yazyev, O.; Austin, A. J.; Cammi, R.; Pomelli, C.; Ochterski, J. W.; Ayala, P. Y.; Morokuma, K.; Voth, G. A.; Salvador, P.; Dannenberg, J. J.; Zakrzewski, V. G.; Dapprich, S.; Daniels, A. D.; Strain, M. C.; Farkas, O.; Malick, D. K.; Rabuck, A. D.; Raghavachari, K.; Foresman, J. B.; Ortiz, J. V.; Cui, Q.; Baboul, A. G.; Clifford, S.; Cioslowski, J.; Stefanov, B. B.; Liu, G.; Liashenko, A.; Piskorz, P.; Komaromi, I.; Martin, R. L.; Fox, D. J.; Keith, T.; Al-Laham, M. A.; Peng, C. Y.; Nanayakkara, A.; Challacombe, M.; Gill, P. M. W.; Johnson, B.; Chen, W.; Wong, M. W.; Gonzalez, C.; Pople, J. A. *Gaussian 03*; Gaussian, Inc.: Wallingford, CT, 2004.
(51) Krisch, M. J.; D'Auria, R.; Brown, M. A.; Tobias, D. J.; Hemminger, J. C.; Ammann, M.; Starr, D. E.; Bluhm, H. *J. Phys. Chem. C* **2007**, *111*, 13497–13509.
(52) Case, D. A.; Darden, T.; Cheatham, I. T. E.; Simmerling, C. L.; Wang, J.; Duke, R. E.; Luo, R.; Merz, K. M.; Wang, B.; Pearlman, D. A.; Crowley, M.; Brozell, S.; Tsui, V.; Gohlke, H.; Mongan, J.; Hornak, V.; Cui, G.; Beroza, P.; Schafmeister, C.; Caldwell, J. W.; Ross, W. S.; Kollman, P. A. *Amber*, 8th ed.; University of California: San Francisco, CA, 2004.
(53) Chang, T.-M.; Dang, L. X. *J. Phys. Chem. B* **2005**, *109*, 5759–5765.
(54) Stewart, E.; Shields, R. L.; Taylor, R. S. *J. Phys. Chem. B* **2003**, *107*, 2333–2343.
(55) Tarek, M.; Tobias, D. J.; Klein, M. L. *Physica A* **1996**, *231*, 117–122.
(56) Taylor, R. S.; Garrett, B. C. *J. Phys. Chem. B* **1999**, *103*, 844–851.
(57) Taylor, R. S.; Ray, D.; Garrett, B. C. *J. Phys. Chem. B* **1997**, *101*, 5473–5476.
(58) Socrates, G. *Infrared and Raman Characteristic Group Frequencies-Tables and Charts*, 3rd ed.; John Wiley & Sons: New York, 2001.
(59) Jayne, J. T.; Duan, S. X.; Davidovits, P.; Worsnop, D. R.; Zahniser, M. S.; Kolb, C. E. *J. Phys. Chem.* **1991**, *95*, 6329–6336.
(60) Fournier, F.; Dubost, H.; Carrez, S.; Zheng, W.; Bourguignon, B. *J. Chem. Phys.* **2005**, *123*, 184705/1–184705/7.
(61) Aqueous Solubility and Henry's Law Constants of Organic Compounds. In *CRC Handbook of Chemistry and Physics*, 88th ed.;Lide, D. R., Ed.; Taylor and Francis: Boca Raton, FL, 2007−2008.
(62) Sander, R. Compilation of Henry's Law Constants for Inorganic and Organic Species of Potential Importance in Environmental Chemistry; 1999.
(63) Dozova, N.; Krim, L.; Alikhani, M. E.; Lacome, N. *J. Phys. Chem. A* **2005**, *109*, 10273–10279.
(64) Wang, W.; Tian, A.; Wong, N.-B. *J. Phys. Chem. A* **2005**, *109*, 8035–8040.
(65) *Computational Chemistry Comparison and Benchmark DataBase*; National Institute of Standards and Technology, 2006.
(66) Fileti, E. E.; Canuto, S. *Int. J. Quantum Chem.* **2005**, *104*, 808–815.
(67) *Physical Constants of Organic Compounds*, 87th ed.; Lide, D. R., Ed.; Taylor and Francis: Boca Raton, FL, 2007.
(68) Lu, R.; Gan, W.; Wu, B.-H.; Zhang, Z.; Guo, Y.; Wang, H.-F. *J. Phys. Chem. B* **2005**, *109*, 14118–14129.
(69) Cordroch, W.; Möbius, D. *Thin Solid Films* **1992**, *210−211*, 135–137.
(70) Goncalves da Silva, A. M.; Guerreiro, J. C.; Rodrigues, N. G.; Rodrigues, T. O. *Langmuir* **1996**, *12*, 4442–4448.
(71) Chen, B.; Siepmann, J. I.; Klein, M. L. *J. Am. Chem. Soc.* **2002**, *124*, 12232–12237.

JP808630V